HYDROLOGICAL PROCESSES
Hydrol. Process. **30**, 2000–2013 (2016)
Published online 28 January 2016 in Wiley Online Library
(wileyonlinelibrary.com) DOI: 10.1002/hyp.10769

Simulated water budget of a small forested watershed in the continental/maritime hydroclimatic region of the United States

Liang Wei,[1*,†] Timothy E. Link,[1] Andrew T. Hudak,[2] John D. Marshall,[1,3] Kathleen L. Kavanagh,[1,4] John T. Abatzoglou,[5] Hang Zhou,[5] Robert E. Pangle[6] and Gerald N. Flerchinger[7]

[1] *Department of Forest, Rangeland, and Fire Sciences, University of Idaho, Moscow, ID, 83844, USA*
[2] *USDA Forest Service Rocky Mountain Research Station, 1221 S. Main St, Moscow, ID, 83843, USA*
[3] *Department of Forest Ecology and Management, Swedish Agricultural University, Skogmarksgränd, Umeå 90736, Sweden*
[4] *Department of Ecosystem Science and Management, 305 Horticulture and Forest Science, Building, MS 2138, College Station, TX, 77843-2138, USA*
[5] *Department of Geography, University of Idaho, Moscow, ID, 83844, USA*
[6] *Department of Biology, University of New Mexico, Albuquerque, NM, 87131, USA*
[7] *USDA Agricultural Research Service, Northwest Watershed Research Center, 800 Park Boulevard, Suite 105, Boise, ID, 83712, USA*

Abstract:

Annual streamflows have decreased across mountain watersheds in the Pacific Northwest of the United States over the last ~70 years; however, in some watersheds, observed annual flows have increased. Physically based models are useful tools to reveal the combined effects of climate and vegetation on long-term water balances by explicitly simulating the internal watershed hydrological fluxes that affect discharge. We used the physically based Simultaneous Heat and Water (SHAW) model to simulate the inter-annual hydrological dynamics of a 4 km^2 watershed in northern Idaho. The model simulates seasonal and annual water balance components including evaporation, transpiration, storage changes, deep drainage, and trends in streamflow. Independent measurements were used to parameterize the model, including forest transpiration, stomatal feedback to vapour pressure, forest properties (height, leaf area index, and biomass), soil properties, soil moisture, snow depth, and snow water equivalent. No calibrations were applied to fit the simulated streamflow to observations. The model reasonably simulated the annual runoff variations during the evaluation period from water year 2004 to 2009, which verified the ability of SHAW to simulate the water budget in this small watershed. The simulations indicated that inter-annual variations in streamflow were driven by variations in precipitation and soil water storage. One key parameterization issue was leaf area index, which strongly influenced interception across the catchment. This approach appears promising to help elucidate the mechanisms responsible for hydrological trends and variations resulting from climate and vegetation changes on small watersheds in the region.

KEY WORDS streamflow; transpiration; LiDAR; sap flux; soil water storage; model test

Received 27 March 2015; Accepted 3 December 2015

INTRODUCTION

Decreasing trends in streamflow have been observed since the 1940s across the Pacific Northwest (PNW), USA (Kalra *et al*., 2008; Luce and Holden, 2009), with the largest declines for the driest quartile of years. This trend may be explained by increased evapotranspiration because of elevated temperatures (Mote, 2003; Walter *et al*., 2004; Abatzoglou *et al*., 2014), or reduction in the proportion of precipitation falling as snow (e.g. Abatzoglou, 2011) and subsequent impacts on streamflow (Berghuijs *et al*., 2014). Alternatively, the decline in annual streamflow may be attributable to a hypothesized decline in orographic precipitation enhancement because of the observed decline in regional lower-tropospheric westerly winds during winter (Luce *et al*., 2013). Despite the general decrease in annual streamflow observed across the PNW, a 33% increase in streamflow has been documented from 1939 to 2012 in the Benton Basin within the Priest River Experimental Forest (PREF) (Hatcher and Jones, 2013; Tinkham *et al*., 2015) despite no discernible change in precipitation (Tinkham *et al*., 2015).

The causes of both decreasing and increasing streamflow trends in mountain basins can be effectively addressed by the application of well-validated, physically based numerical models that can explicitly simulate both climate and vegetation dynamics with a minimum of calibrated parameters. There are a number of models that operate over raster grids (e.g. DHSVM; Wigmosta *et al*., 2002) or triangular irregular networks (e.g. PIHM; Kumar *et al*., 2009) that can very effectively simulate intra-annual streamflow dynamics in small complex watersheds. There is a need for modelling approaches that provide a simpler hydrologic response unit (HRU) based

*Correspondence to: Liang Wei, Department of Forest, Rangeland, and Fire Sciences, University of Idaho, Moscow, ID 83844, USA.
E-mail: liangwei@uidaho.edu
†Current Address: Department of Forestry, University of Missouri, Columbia, MO, 65211, USA

representation of complex terrain without sacrificing process representation. These models can address questions focused on how specific watershed and climate characteristics affect hydrological processes and hence controls on longer-term inter-annual variations. In addition, these modelling exercises benefit the development of regional parameterization approaches (e.g. CRHM; Fang *et al.*, 2013) to advance our understanding of how these processes are likely to affect these fluxes at other catchments in the region.

Although detailed grid-based approaches can be used to simulate long-term interannual flow variations (e.g. Du *et al.*, 2014), simpler approaches that aggregate water balance components at the HRU scale are an effective means to estimate streamflows in complex terrain (e.g. Chauvin *et al.*, 2011) if they include sufficient process detail for the question being investigated. In order for such simple approaches to be effective, the internal watershed processes simulated by the model must be validated individually (Thyer *et al.*, 2004) to enable the assessment of hydrological changes over long-term periods. Data from multi-disciplinary research sites may be used to parameterize and validate relatively simple physically-based modelling approaches to address hydrological questions such as long-term flow changes in complex terrain that is subject to both changing vegetation and climate conditions. It is hence highly advantageous from both the research and management perspectives to simulate hydrological dynamics with minimally calibrated physically based models to ensure that correct answers are obtained for the correct reasons (Kirchner, 2006).

The general objective of this study was to evaluate the strengths and weaknesses of a relatively simple modelling approach to estimate annual water balance components in a mountainous watershed comprised of a mix of forest conditions. Specific objectives were to: (1) develop parameterizations to effectively simulate snow, transpiration, and soil water content (SWC) dynamics at the HRU level, (2) assess the potential to aggregate simulated runoff and deep drainage fluxes from HRUs as a proxy for annual runoff, and (3) assess the range of interannual variations in the major components of the water balance between HRUs with distinctly different topographic and vegetation characteristics. The outcome of this work is to provide information on how well a relatively simple modelling approach can be used to simulate the water balance components in a complex mountainous watershed to address questions about how climate and landcover changes affect annual runoff.

METHODS

Model description

We used the physically based Simultaneous Heat and Water (SHAW) model (Flerchinger *et al.*, 1990; Flerchinger *et al.*, 1996; Flerchinger *et al.*, 1998), to estimate the water budget in the Benton Basin. SHAW simulates the major components of the water budget based on fundamental physical processes that control hydrological dynamics including: precipitation, snowpack development and ablation, evaporation, transpiration, soil moisture redistribution, deep percolation, and runoff. The SHAW model has been rigorously tested in various environments (Flerchinger and Cooley, 2000; Flerchinger *et al.*, 2003; Link *et al.*, 2004a; Campbell *et al.*, 2010), making it feasible to apply at Benton Basin.

The SHAW model is a one-dimensional hydrological model, which was originally designed to simulate soil freezing and thawing (Flerchinger and Saxton, 1989a,b; Flerchinger *et al.*, 1990). Plant components were later added to estimate the heat and water movement through a multiple-species canopy (Flerchinger and Pierson, 1991; Flerchinger *et al.*, 1996) and modified to accurately simulate forest water dynamics (Link *et al.*, 2004a; Flerchinger *et al.*, 2015). SHAW now simulates the transfer of heat, liquid water, and water vapour through a plant–snow–residue–soil system. Detailed description and numerical implementation of SHAW can be found in many prior publications, including Flerchinger *et al.* (1996), Flerchinger *et al.* (1998), Link *et al.* (2004a), and Chauvin *et al.* (2011).

The water balance is described in SHAW as (Flerchinger *et al.*, 1998):

$$P = E + T + \Delta S + R + DP \tag{1}$$

where: P is precipitation, E is evaporation (mainly canopy interception), T is transpiration, ΔS is change in storage, R is runoff, and DP is deep percolation. Transpiration is a major component in the water budget, especially in forested mountain regions. Soil water status and ambient vapour pressure strongly affects the stomatal conductance (g_s) of plants in SHAW through its influence on leaf water potential, and hence controls transpiration. SHAW additionally includes a simplified Jarvis–Stewart model to simulate ambient vapour pressure deficit (VPD) controls on stomatal conductance as formulated by Ogink-Hendriks (1995) and incorporated into the SHAW model by Link *et al.* (2004a):

$$f(VPD) = K_{VPD} + (1 - K_{VPD})r^{VPD} \tag{2}$$

where $f(VPD)$ is the reduction factor (0–1, dimensionless) for g_s, K_{VPD} is the maximum g_s reduction at high VPD, and r is a constant. This function is important for the accurate simulation of hydrological processes in seasonally arid forests, because ambient humidity can be more limiting than soil moisture for forest transpiration, especially in early summer when SWC is high, but ambient humidity levels can be low (Link *et al*., 2004a; Wei *et al*., 2014).

Study site

The PREF is located in the northern Rocky Mountains in northern Idaho (48° 45′N, 116° 49′W) (Figure 1). Elevation ranges from 675 m (west) to 1825 m (east) (Pangle *et al*., 2015). Annual precipitation ranges from 812 mm at low elevations to 1270 mm at higher elevations (Finklin, 1983). The soil is comprised of a silt-loam surface layer, a silty clay loam subsoil, and a deeper soil of gravelly to very gravelly sands and sandy loams (Page-Dumroese, 1993). Benton Basin is 4 km^2 in area and occupies the south-central portion of PREF (Figure 1). Benton Creek flows from east to west, and is generally comprised of north and south facing slopes except for some west-facing slopes near the headwaters. Benton Creek begins at the perennial Benton Spring and flows 3.25 km to reach the Benton Dam, a gauging station comprised of a compound weir where streamflow has been monitored since 1939 (Stage, 1957).The Benton Basin within PREF is an ideal place to study the impact of climate and landcover changes on water budgets in PNW. PREF has a comprehensive record of climate, forest growth, and landcover changes (e.g. logging, road construction, forest thinning), Many physiological features of the forest and hydrological fluxes have been measured (e.g. leaf area index, transpiration, and specific leaf area, Duursma *et al*., 2003; Pangle *et al*., 2015), which help to constrain the parameterizations for simulation of hydrological processes.

Ten conifer species common in the northern Rockies are well represented at PREF and include (listed in order of dominance): western red-cedar (*Thuja plicata* Donn ex D. Don), Douglas-fir (*Pseudotsuga menziesii* var. *glauca* (Beissn.) Franco), western hemlock (*Tsuga heterophylla* (Raf.) Sarg.), western larch (*Larix occidentalis* Nutt.), grand fir (*Abies grandis* Douglas ex D. Don Lindl.), lodgepole pine (*Pinus contorta* Douglas ex Loudon), subalpine fir (*Abies lasiocarpa* (Hook.) Nutt.), western white pine (*Pinus monticola* Dougl. ex D. Don), ponderosa pine (*Pinus ponderosa* Dougl. ex Laws.), and Engelmann spruce (*Picea engelmannii* Parry ex Engelm) (Duursma *et al*., 2003; Duursma *et al*., 2007). Western redcedar, Douglas-fir, and western hemlock (listed in order of prevalence) currently comprise 70% of forest basal area (Duursma *et al*., 2003).

Hydrometeorological data

We ran SHAW from 2003 to 2010 with daily weather data including maximum (T_{max}) and minimum (T_{min}) air temperature, dewpoint temperature, mean wind speed, solar radiation, and precipitation. Meteorology data from 16 stations were used to drive the SHAW model (Figure 1, Table I), and the specific approach is discussed in the 'Model implementation' section below. Station WS1 (Figure 1, Table I), had the most complete record and we hence ran the SHAW model in accordance with the WS1 complete observation period (September, 2003–June,

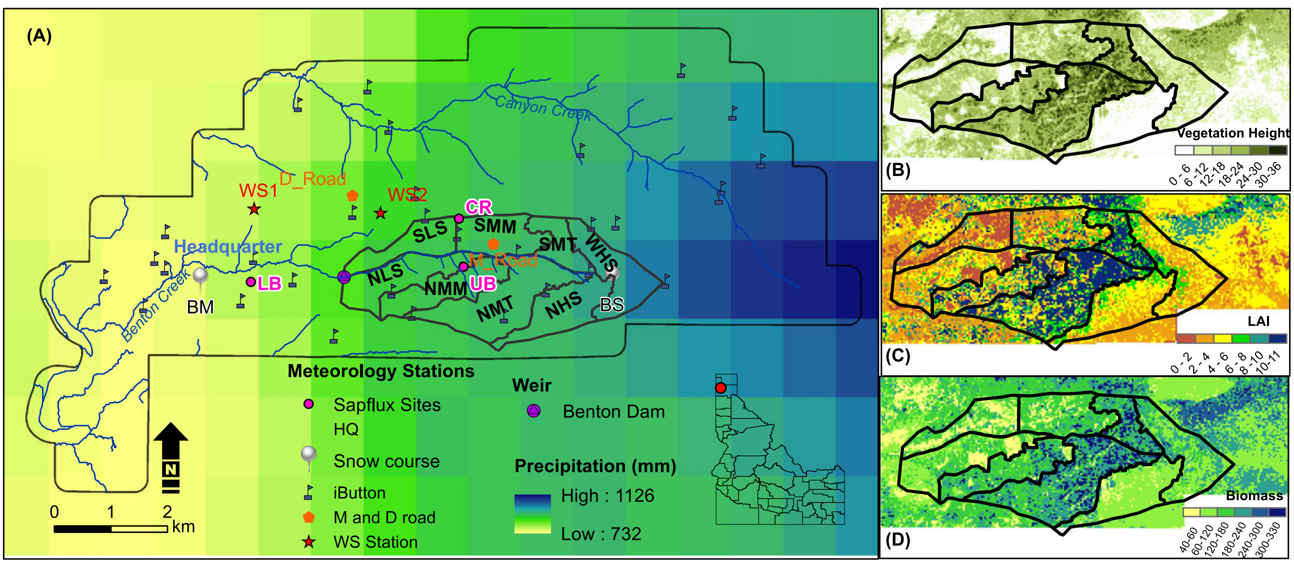

Figure 1. Strata for model simulations and locations for observation sites. A weir has been measuring streamflow from Benton Basin since 1939. Benton Basin is divided into eight HRUs (outlined in black) for SHAW modeling based on elevation, aspect, and vegetation within the Benton Basin (see Table II). Outer boundary outlines the Priest River Experimental Forest (PREF). Locations of weir and weather stations are shown in Figure 1A, along with annual precipitation of a sample year (water year 2007), which was estimated using PRISM. See Table I for descriptions of each meteorological station. Vegetation height (m) (Figure 1B), LAI (Figure 1C), and aboveground biomass (Mg ha^{-1} of dry mass) (Figure 1D) are derived from LiDAR estimates. The spatial resolution was 1/120° of latitude and longitude for precipitation map, and 20 m for LAI, vegetation height, and biomass

Table I. Description of meteorological stations (see Figure 1 for locations). Check signs (√) indicate available data at a given station. Abbreviations: T = air temperature, Wind = wind speed, RH = relative humidity, Solar = solar radiation, SWE = snow water equivalent

Station name	*N* of sites used(total)	Duration	T	RH	Wind	Solar	Snow depth	SWE
WS1 and WS2	2	17 Sep 2003–20 Jun 2010	√	√	√	√		
M and D road	2	1998–present	√	√	√			
Sapflux	3	19 Jun 2003–8 Nov 2005	√	√	√			
iButtons	8 (29)	2 Oct 2010–present	√					
Headquarter, NCDC	1	1911–present	√				√	
Snow Course	2	1936–present					√	√

2010), which included six entire water years (2004–2009, i.e. Oct. 2003–Sep. 2009). We also used the records from WS1 to extend the temporal temperature records of stations within the Benton Basin.

Air temperatures were observed at all stations but not all of them had complete records from 2003 to 2010 (Table I). Missing observations were infilled using multiple linear regressions between stations, and the Akaike information criterion (AIC) was applied to pick the best multiple linear regression model. Absolute humidity was very similar (i.e. the slopes of linear regressions between WS1 and other stations were not different from 1 and the intercepts were not different from 0, $\alpha = 0.05$) across the seven stations within PREF (Table I) and hence we used data from the station with the longest record (WS1) to represent the PREF. Wind speed and solar radiation were observed at multiple stations in PREF (Table I), but we used only one station as the reference for wind and another for solar radiation, because of data quality or completeness relative to other stations (see Model implementation below).

We estimated gridded daily precipitation based on monthly data from the Parameter–elevation Relationships on Independent Slopes Model (PRISM; Daly *et al*., 1994; Daly *et al*., 1997). PRISM accounted for the spatial variability in precipitation because of topography within in PREF to provide data at ~800-m horizontal resolution. Daily precipitation data at the HQ station situated along Benton Creek 2 km downstream of the Benton Basin streamflow gauging station were used to temporally disaggregate monthly PRISM precipitation totals to daily values by applying daily ratios of accumulated monthly precipitation at the HQ station to the PRISM grid.

Snow depth and snow water equivalent (SWE) data were measured at multiple locations and used as a diagnostic variable to test and improve model performance. Snow depth has been measured at the HQ station (725 m a.s.l.) since 1911. Snow depth and SWE have been measured at the Benton Meadow (BM, 725 m) and Benton Spring (BS, 1455 m) snowcourses within Benton Basin since 1936 (http://www.wcc.nrcs.usda.gov/nwcc/rgrpt?state=ID&report=snowcourse) (Figure 1).

Soil measurements

Soil moisture and temperature were measured at seven forested sites within Benton Basin and used to diagnose model performance (locations not shown). Soil temperature was measured at 0, 5, 10, and 20 cm below the litter surface using thermocouples (Omega Engineering, Stanford, CT, USA) and soil moisture at 10, 20, and 40 cm below the litter surface using frequency domain capacitance probes (EC-10, Decagon Devices, Pullman, WA, USA) (Berryman *et al*., 2014).

Soil texture (% sand, silt, and clay), soil organic matter content, and bulk density were measured at nine stations across PREF (locations not shown) to parameterize the model. Soil texture and soil organic matter content were measured at five depths (10, 30, 50, 70, and 90 cm) and dry bulk density at three depths (10, 20, and 40 cm).

Sapflux and vegetation dynamics

Sapflux was measured at three sites in PREF from May to October of 2004 and 2005 (Kavanagh *et al*., 2007; Pangle *et al*., 2015), and used to refine the parameterization of the model. The sapflux sites are Lower Benton (LB), Upper Benton (UB), and Center Ridge (CR) (Figure 1, magenta labels). Each site included three stands and each stand represented short (S), intermediate (I), and tall (T) tree height classes (short 7.3 m (standard error, SE, 1.4), intermediate 20.9 m (1.1), and tall 31.5 m (0.9); SE indicates the variation within sites). A total of 50 trees were instrumented within the nine stands, including Douglas-fir, western hemlock, western larch, western red-cedar, and western white pine. The tree-level observations were upscaled to the stand level (Pangle, 2008), to compare to the model simulations.

SHAW parameters for vegetation characteristics and dynamics were obtained from field and airborne LiDAR data collections from 2002. These parameters included vegetation height (m), leaf area index (LAI, $m^2\ m^{-2}$), and aboveground biomass ($Mg\ ha^{-1}$ of dry mass) (Table II). LAI and biomass (Figure 1 and Table I) were imputed based on plot-level allometric LAI measurements and

Table II. Properties of eight HRUs (see Figure 1 for locations) used for model simulations. LiDAR provided the means to map vegetation height, LAI, aboveground biomass, and changes in these variables (i.e. Δ height, ΔLAI, Δ biomass) between 2002 and 2011 (see text for details). Biomass growth (Δ biomass) was obtained from 10-year tree ring width (1992–2001) (Duursma *et al.*, 2003; Duursma *et al.*, 2007), and we assumed a similar growth rate during our simulation period. Parenthetical values show the range of elevation, and the standard deviation (SD) of LAI and height within each HRU

HRU	Vegetation height class	Area (km^2)	Elevation (m)	Slope (°)	Aspect (°)	Vegetation height (m)	ΔHeight ($m\,year^{-1}$)	LAI ($m^2\,m^{-2}$)	ΔLAI ($m^2\,m^{-2}\,year^{-1}$)	Aboveground biomass ($Mg\,ha^{-1}$)	ΔBiomass ($Mg\,ha^{-1}\,year^{-1}$)
SLS	Short	0.39	1001 (805–1153)	25	200	12.8 (6.9)	0.41	3.4 (2.6)	0.23	109.2	2.6
SMM	Medium	0.44	1163 (995–1307)	24	210	18.2 (5.3)	0.37	5.4 (2.8)	0.23	149.6	4.8
SMT	Tall	0.25	1290 (1145–1380)	23	240	23.4 (4.4)	0.28	8.5 (2.5)	0.06	213.1	4.3
WHS	Short	0.53	1506 (1323–1700)	21	270	13.0 (3.6)	0.37	4.8 (1.7)	0.00	143.2	3.2
NLS	Short	0.54	978 (803–1093)	25	330	13.3 (4.7)	0.32	4.3 (2.5)	0.34	114.7	2.6
NMM	Medium	0.48	1105 (1048–1167)	19	320	19.7 (5.4)	0.31	6.9 (3.2)	0.13	175.8	4.3
NMT	Tall	0.87	1222 (1073–1373)	19	320	25.4 (4.8)	0.34	8.6 (2.9)	0.06	211.7	4.3
NHS	Short	0.51	1394 (1270–1505)	22	330	8.7 (4.4)	0.36	4.8 (1.5)	0.17	114.2	3.2

canopy height and density metrics calculated from the LiDAR data within the same 35 field plots (Eskelson *et al.*, 2009). The imputation model was then applied to the same LiDAR metrics, to generate gridded 20 m LAI and biomass maps for 2002 following the approach of Hudak *et al.* (2008) for biomass mapping. The same model was also applied to the same gridded LiDAR metrics generated from a 2011 LiDAR collection, to produce updated LAI and biomass maps (Fekety *et al.*, 2015). Thus, the 2002 and 2011 LAI and biomass maps across PREF effectively bracketed the 2003–2010 period used to parameterize SHAW.

Stream discharge

Streamflow has been recorded at Benton Dam since 1939 and was used to assess the performance of the simulated potential streamflow. The concrete dam extends to bedrock, and two trapezoidal Cipolletti weirs are embedded in the dam (Stage, 1957). Water flows perennially through the smaller weir with a 1-foot (0.3048 m) crest; when the streamflow is high and the head exceeds 0.75 feet, water flows through a larger weir with a 10-foot crest. The water level is measured in a stilling well connected to the pond above the dam. Different recording devices have been used over the length of record. A Stevens water-stage recorder with mechanical strip charts was used in the early years (Stage, 1957); electronic devices were added in 1993 and completely replaced the mechanical device in 2006 with electronic water level sensor (Magna-Rule sensor) connected to CR10 datalogger (Campbell Scientific, Logan, UT, USA). Streamflow data and background information are available online at 10.2737/RDS-2015-0006 (Link *et al.*, 2015).

Model implementation

The SHAW Model was used to estimate the monthly and annual water balance of the Benton Basin by running the model with discrete sets of landscape parameters and hydrometeorological variables corresponding to eight hydrological response units (HRUs). A similar approach was successfully used to simulate long-term annual water balances of a small watershed comprised of three HRUs (Chauvin *et al.*, 2011; Flerchinger and Cooley, 2000), but has not been applied to a watershed with this level of complexity. This approach was selected to balance reasonable simulation of the landscape complexity with a minimum of landscape classes for efficiency of parameterization and computation.

Eight HRUs were defined by aspect (S = south, W = west, N = north), elevation (L = low, M = mid, H = high), and vegetation height (S = short, M = medium, T = tall) classes (Figure 1, Table II). Each three-letter HRU code corresponds to each variable respectively—e.g.: SLS = South-facing, Low-elevation, Short canopy class. Not all combinations of aspect, elevation, and vegetation classes are present in the basin given the specific physiography and land use history. HRU boundaries closely (but not strictly) follow topographic contours, but with a few small deviations to reflect long-established boundaries between young and old stands, as apparent from aerial imagery (Figure 1). Based on LiDAR data, four HRUs in short vegetation classes (SLS, WHS, NLS, and NHS) had mean tree heights ≤ 13.3 m, and mean LAIs ≤ 4.8; medium-height classes (NMM and SMM) had mean tree heights from 18.2 to 19.7 m and mean LAIs of 5.4–6.9; and the tall classes (NMT and SMT) had mean tree heights ≥ 23.4 m and LAIs ≥ 8.5. The aboveground biomass was also the highest in the tall vegetation class and lowest in the low vegetation class as expected. These estimated HRU properties (Table II) were used as defining parameters for each simulation.

We treated each HRU as a homogenous unit, and one set of hydrometeorological variables was applied to each HRU. In some cases hydrometeorological variables were identical across HRUs, and in some cases differed between HRUs depending on data availability and typical variations of climate in complex terrain. T_{min}, T_{max}, and precipitation differed between the HRUs. If there was a station that was located approximately at the central elevation within an HRU, we applied the temperatures of that station to the HRU; otherwise, we computed the means from two stations that bracketed the elevation of that HRU. Daily precipitation for each HRU was the mean of the PRISM values weighted by the area of PRISM grid cells inside the HRU boundary. Identical dewpoint temperatures were applied to all HRUs because measured absolute humidities at seven stations in PREF (Table I) were very similar. Although wind speeds were measured at multiple stations in PREF, within the Benton Basin wind speed was only measured above the canopy at the CR sapflux site which was therefore applied to the entire Benton Basin. Because there were only two years of data at the CR site, we extended the wind speed using linear regressions between site CR and WS1, where the longest record of wind speed was recorded within the Benton Basin ($P < 0.01$, adj.$R^2 = 0.64$).

Shortwave radiation was recorded at station WS1, but daily trends indicated that surrounding vegetation intercepted too much of the incoming radiation. We therefore estimated shortwave radiation based on extra-terrestrial shortwave radiation adjusted for slope, aspect, and local daily cloud factors (Wei *et al.*, 2014). Cloud factors were estimated as ratios of measured to calculated extraterrestrial shortwave radiation at Deer Park, WA (National Solar Radiation Data Base, NSRDB. Station number: 727854), 65 km southwest of PREF. This station was chosen because of its proximity to PREF and its similar elevation to reference station WS1. Daily solar radiation at the Deer Park station also had the highest correlation ($P < 0.001$, $R^2 = 0.90$) with WS1 among five NSRDB stations in an approximately 200-km radius. This indicated similar levels of cloudiness between Deer Park and WS1. Shortwave radiation was then estimated based on the computed cloud factors and mean slope and aspect for each HRU (Table II).

Temporal variation in LAI change was estimated from LiDAR data following the methodology of Hudak *et al.* (2012), and the imputed LAI map of 2002 was subtracted from 2011 map to produce a map of LAI change between the two LiDAR acquisition dates. The change in LAI was notably noisy at the scale of individual grid cells but produced reasonable LAI estimates when aggregated to the scale of each HRU (Figure 1). Mean height growth was 0.28–0.41 m year^{-1} and mean LAI change was 0.00–0.34 m^2 m^{-2} year^{-1} from 2002 to 2011 among the eight HRUs. We assumed a linear change in vegetation height and LAI from 2002 to 2011 to simulate the vegetation growth in SHAW; there were no stand-replacing disturbances within Benton basin during this period.

The changes in aboveground biomass were obtained from field measurements for our simulation period (Duursma *et al.*, 2007). Forest stands were measured at 35 sites across PREF, and increment cores were collected from 619 out of 1238 trees in 2002; 10-year growth (1992–2002) was then estimated for those sites based on tree ring data (Duursma *et al.*, 2007). We searched the pool of field plots ($n = 35$) to identify the closest matches of mean height and aboveground biomass to the HRUs. We then assumed that the mean annual growth rate in an HRU was the same as its corresponding plot(s). We finally applied the mean annual biomass increment of the corresponding site to the HRU as a SHAW parameter.

Model parameterization

The primary objective of this research was to assess the performance of a relatively simple, minimally-calibrated modelling approach to simulate the water balance of a complex, forested, mountain watershed. Our approach was therefore to use measured parameter values wherever possible, and reasonable estimated or default values if measurements were not available. Estimated and default parameters were subsequently refined based on measured internal watershed data including snowpack, soil moisture, stomatal conductance, and transpiration (see below) to effectively tune the model (see Table A1). Parameters derived from on-site measurements were refined to enhance the performance of simulated internal states and fluxes. This light calibration approach was an effective means to approach questions related to spatial variations in land cover and climate changes in complex terrain (Kirchner 2006). We did not adjust any parameters to fit either the simulated soil temperatures or streamflow to observations.

Although the temperature where there is equal probability of snow and rain was found to be 1.2 °C for land (Dai, 2008), the most effective snow depth simulations resulted when the threshold temperature for snowfall (T_i) was set to 0 °C at site HQ. This same threshold was used as a long-term indicator of precipitation phase at other mountainous sites (Marks *et al.*, 2013). Below T_i, the precipitation was considered as only snow and above it as only rain.

Precipitation interception is simulated by SHAW based on the maximum amount of precipitation intercepted and stored per unit leaf area index (S_c). This parameter was estimated from high resolution throughfall measurements (Leyton *et al.*, 1967; Gash, 1979; Link *et al.*, 2004b) in a forest with similar species at the Mica Creek Experimental Watershed (Wei *et al.*, 2014), located 130 km south of PREF. The saturation storage of the canopy was estimated to be 2.15 mm in a stand with LAI = 7.0 (Wei *et al.*, 2014). This was generalized as $S_c = 0.31$ mm per unit LAI.

Simulated transpiration was calibrated based on stand-scale estimates derived from sapflux measurements collected throughout PREF (Pangle *et al.*, 2015). We implemented the model with identical values of parameters that control transpiration dynamics for all eight HRUs except for minimum stomatal resistance (r_{s0}, the reciprocal of maximum stomatal conductance), which differed by height class (Table A1). We calibrated r_{s0} by fitting the simulated transpiration to the mixed-species, stand-level transpiration estimates (Pangle *et al.*, 2015). This approach was simpler than calibrating each individual species and aggregating to the stand level. The r_{s0} parameter was calibrated at one HRU for each vegetation height class (Figure 3), and the same value was then applied to all HRUs with similar height classes (Table A1). We calibrated the simulated transpiration for the NMT HRU with observations at the Upper Benton Tall canopy (UB-T) plot, NLS with the Lower Benton Short canopy (LB-S) plot, and NMM with the Upper Benton Intermediate canopy (UB-I) plot. We applied the mean estimated values of the parameters that control the stomatal response to VPD ($K_{VPD} = 0.10$, $r = 0.36$; Equation (2)) from nine stands for all HRUs. The K_{VPD} and r values were estimated by fitting Equation (2) based on the observed VPD and stomatal conductance at each plot.

Stomatal conductance and thus transpiration are reduced following exposure to freezing temperatures (Smith *et al.*, 1984). Because SHAW does not consider the impact of freezing temperatures on the subsequent day's transpiration (Wallin *et al.*, 2013) we set the initiation of transpiration at 8 °C. This prevented transpiration in February and March when the nighttime temperatures were consistently below freezing and photosynthesis and transpiration should not be occurring because of stomatal closure.

Most soil parameters were obtained from measurements (Table A1). We applied the mean soil texture (% sand, silt, and clay), soil organic matter content, and bulk density properties from nine sampling locations to all HRUs (Table A1). Saturated volumetric water content (θ_s) in SHAW was set as the highest measured soil moisture value for each layer (Table A1), and θ_s for soil depths exceeding 40 cm was set to the value for the 40 cm depth.

The saturated conductivity (K_s), air-entry potential (Ψ_e), and Campbell's pore-size distribution index (b) were calibrated to best fit simulated soil moisture to the mean value observed at seven forested sites inside PREF. The soil properties were only calibrated for the 10-cm layer; identical values for K_s, Ψ_e, and b were applied for all other soil depth layers. This relatively simple approach was taken to estimate the general behaviour of SWC dynamics across the watershed. A detailed parameter adjustment for all layers was not completed as we did not have sufficient data to account for fine scale soil heterogeneity in the vicinity of the probes.

The SHAW model does not simulate streamflow directly, but because the Benton Basin is a steep watershed with relatively shallow soils and impermeable bedrock (Cline *et al.*, 1977), water draining out of the simulated profile as deep percolation is expected to rapidly convert to streamflow. Deep percolation was simulated in SHAW as the water moving between the deepest two soil nodes within the soil profile. Although SHAW only simulates vertical fluxes and does not simulate hydrological routing to or through a stream network, we used the simulated sum of deep percolation and surface runoff to estimate the potential water available for streamflow (Q_{pot}). Based on the catchment characteristics, small spatial scale of the HRUs, and the annual scale of interest, potential streamflows from the combined HRUs were used as a streamflow proxy. Observed annual runoff (Q) at Benton Dam was hence used to independently validate the simulated potential annual runoff from the combined HRUs, similar to the approach used for other small-scale simulation studies (Flerchinger and Cooley, 2000; Chauvin *et al.*, 2011).

Model performance

Model performance was evaluated based on the model efficiency (ME), or Nash–Sutcliffe (1970) coefficient, root-mean-square difference (RMSD), and mean bias difference (MBD). These metrics are defined as follows:

$$ME = 1 - \left(\frac{\sum_{i=1}^{n} (x_{obs} - x_{sim})^2}{\sum_{i=1}^{n} (x_{obs} - x_{ave})^2} \right)$$

$$RMSS = \frac{1}{n}\sqrt{\sum_{i=1}^{n} (x_{sim} - x_{obs})^2}$$

$$MBD = \frac{1}{n}\sum_{i=1}^{n} (x_{sim} - x_{obs}) \quad (3)$$

where n is the number of pairs of compared values, x_{obs} is the observed value, x_{sim} is the simulated value, and x_{ave} is the mean of observed values. ME values range from $-\infty$ to 1; ME = 1 indicates a perfect match between simulations and observations, ME = 0 indicates that the model predicts as accurately as the observed mean, and ME < 0 indicates that the predictions are worse than the observed mean and hence indicates unacceptable model performance. The RMSD and MBD both indicate the agreement between model predictions and observations; values closer to 0 indicate better model performance for these indices.

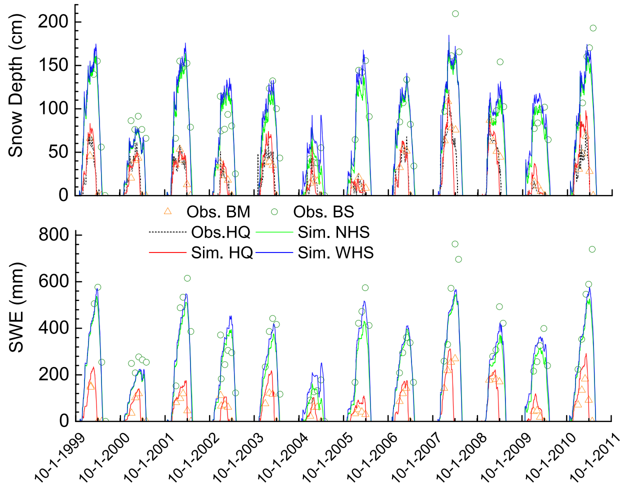

Figure 2. Observed and simulated snow depth and SWE. Simulations are in daily time step. Snow depth was observed hourly at Headquarter (HQ, 725 m a.s.l.) while displayed daily here; snow depth and SWE were observed monthly at two sites (dots): Benton Spring (1455 m), and Benton Meadow (725 m) (see Figure 1). We calibrated the SHAW model at the HQ station by fitting simulated snow depth with observations. After calibration, we compared simulations at hydrologic response unit (HRU) NHS (north-slope high-elevation short-canopy) and WHS (west-slope high-elevation short-canopy) to observations at BS station, which was located at the border between HRU NH and WH

RESULTS

Model simulations

The parameters for site properties are shown in Table II, and the complete set of model parameters is shown in Table A1. A snowfall threshold temperature of 0 °C (T_i) produced the best fit (ME 0.96, MBD −4.77 cm, and RMSD 0.00 cm.) between simulated snow depth and continuous automated observations at the HQ station (Figure 2). Snow depth and SWE simulations were also reasonable when compared to measurements at the Benton Meadow (BM) snow course located close to the HQ measurement site (ME: 0.64 for snow depth and 0.29 for SWE, also see MBD and RMSD in Table III). Simulated snow depths at both the NHS and WHS HRUs exhibited reasonable agreement with both snow depth (ME 0.64, both) and SWE observations (ME 0.50–0.57) at the Benton Spring snow course located between the two HRUs (Figure 2, Table III). The relatively large discrepancies and negative biases between the simulated and observed values (Table III) were not unexpected because the snow course is located on a relatively flat, sheltered road cut, whereas the simulated values are for sloping sites with a short canopy cover. These differences are likely responsible for the apparent underestimation of SWE at the HRUs during most years because the measurement site accumulates more SWE than the forested areas because of reduced canopy interception losses. These results indicate that the parameterization based on measurements at HQ produced reasonable snow simulations at higher elevations in the watershed and was therefore appropriate for the objectives of this study.

Figure 3 shows simulated daily transpiration and estimates derived from measurements of sap flux in different canopy height classes within and in the near vicinity of the watershed. The maximum stomatal conductance was adjusted for each height class to minimize temporally integrated differences between the simulated and observed values at the most analogous HRUs and measurement sites (Table III). The model reasonably simulated daily variations in transpiration at these sites within the different height classes with MEs ranging from 0.47 to 0.72. Sites with relatively low observed sapflux values in the short stands were typically characterized by relatively low LAI values (e.g. CR-S, LAI 2.3) relative to the simulated HRU conditions. The model over-predicted transpiration in the tallest height classes (e.g. LB-T and CR-T, Figure 3C); however, these sites were taller than any of the simulated HRU conditions. Comparison of observed sapflux data between different locations (Pangle *et al.*, 2015) indicates that simulated variations within each tree height class were smaller relative to measured values. This is most likely related to smaller variations in the LAI and vegetation height of our HRUs relative to sapflux sites in each tree height class.

The model reasonably simulated the SWC dynamics during the mid-winter period, as well as the July–August, 2006 summer period (Figure 4, Table III). Maximum

Table III. Model performance statistics (see Equation (3)). The better the model performs, the closer the ME value to 1 and MBD value to 0, and the smaller the RMSD. Underlined items were calibrated. We did not calibrate any parameters for simulating soil temperature and streamflow and used them as tests of model performance. Transpiration was calibrated at three HRUs (NLS, NMM, and NMT); snow depth was calibrated only at site HQ; and soil moisture was calibrated based on only 10-cm depth data

	N of samples	ME	MBD	RMSD
Transpiration NLS	209 days	0.72	0.07 mm	0.17 mm
Transpiration NMM	188 days	0.58	−0.02 mm	0.27 mm
Transpiration NMT	155 days	0.47	0.01 mm	0.31 mm
Snow depth, HQ *versus* NCDC	2461 days	0.96	−4.77 cm	0.00 cm
Snow depth, HQ *versus* BM	28 days	0.64	−2.94 cm	3.55 cm
Snow depth, WHS *versus* BS	33 days	0.71	−2.44 cm	3.90 cm
Snow depth, NHS *versus* BS	34 days	0.65	−14.78 cm	4.25 cm
SWE, HQ *versus* BM	28 days	0.29	12.84 mm	2.93 mm
SWE, WHS *versus* BS	33 days	0.57	−23.06 mm	14.50 mm
SWE, NHS *versus* BS	34 days	0.50	−62.75 mm	17.47 mm
Streamflow (monthly)	80 months	0.56	2.27 mm	3.04 mm
Streamflow (annual)	6 years	0.62	16.16 mm	16.81 mm
Soil temperature 0 cm	233 days	0.24	−0.32 °C	0.09 °C
Soil temperature 5 cm	233 days	−0.15	−0.60 °C	0.09 °C
Soil temperature 10 cm	233 days	−0.35	−0.67 °C	0.10 °C
Soil temperature 20 cm	233 days	−0.14	−0.61 °C	0.09 °C
Soil moisture 10 cm	341 days	0.79	0.00 $v\ v^{-1}$	0.00 $v\ v^{-1}$
Soil moisture 20 cm	341 days	0.88	0.00 $v\ v^{-1}$	0.00 $v\ v^{-1}$
Soil moisture 40 cm	341 days	0.90	0.00 $v\ v^{-1}$	0.00 $v\ v^{-1}$

simulated SWC was higher during the seasonal moisture state transitions that occurred in November, 2006 and April–June, 2007. Despite these discrepancies, we consider the soil moisture simulations to be reasonable for the purposes of this investigation because our primary objective was to accurately simulate annual hydrological fluxes rather than to optimize simulation of the intra-annual dynamics.

Simulated soil temperature matched the general pattern of observations (Figure 4). However, simulations were less variable in November 2006 and April–June, 2007 than observations. This is likely related to accumulated snow in the simulations (Figure 2), which insulated the ground and hence buffered simulated temperatures relative to the locations where values were measured (see Discussion). This factor coupled with the relatively short evaluation period may have caused the generally low model performance for simulating soil temperature in terms of model efficiency (Table III).

As previously discussed, the SHAW model does not simulate streamflow, but the combined outputs of surface runoff and deep drainage can be defined as potential streamflow (Q_{pot}) used as a proxy for streamflow (Q) over long time periods. Assuming that Q_{pot} can be used as a proxy for Q, the model accurately simulated streamflow means and inter-annual variations (Figure 5B). Model performance statistics also indicated very reasonable model performance (ME 0.62, Table III) considering the relatively simplistic model structure relative to the watershed complexity. Observed mean annual Q was 442 mm, whereas the simulated Q_{pot} was 457 mm from water year 2004 to 2009. The simulated Q_{pot} also generally represented monthly variations in streamflow (Figure 5A) which is indicative of the short lag time between drainage from the simulated profile and streamflow response. The ensemble mean monthly simulated Q_{pot} values were notably higher than Q observations during the high-flux period from April to May but lower during the low-flux period from July to Feb (inset of Figure 5).

Interannual variability

Inter-annual variation for precipitation, streamflow, and soil storage was large in Benton Basin; the range was 348, 235, and 232 mm for these three terms, respectively (Figure 6) in water year 2004–2009. On the other hand, transpiration and canopy interception loss (evaporation) varied little and so had little influence on the water budget; the range was only 39 and 72 mm for transpiration and canopy interception, respectively.

Canopy stratum differences

We estimated differences in annual water budget components between the eight HRUs (Figure 7). Annual mean precipitation ranged from 904 mm in low-elevation HRU NLS to 1001 mm in high-elevation HRU WHS (Figure 7e). Canopy interception had the largest variation (257-mm range) among all components of the water budget, which probably relates to differences in LAI (Figure 7b) and to a lesser extent, total

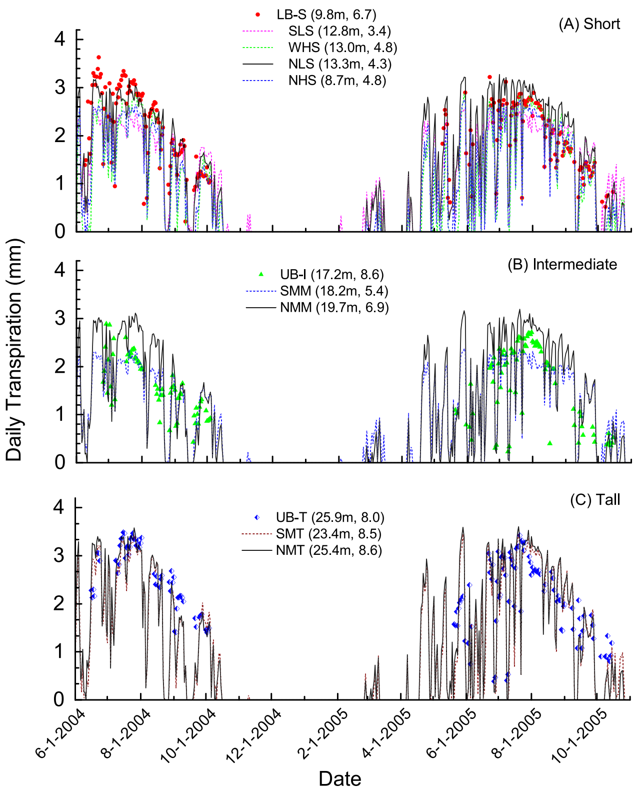

Figure 3. Simulated using SHAW (dashed lines) and measured (dots) daily transpiration based on sap flux measurements in short (a), medium (b), and tall (c) canopy height classes at Priest River Experimental Forest. Numbers in the parentheses of legends indicate vegetation height and leaf area index (LAI), respectively. We calibrated the minimum stomatal resistance value to fit the transpiration of HRU NLS (north-slope low-elevation short-canopy) to plot LB-S (lower Benton short canopy), NMM to plot UB-I (Upper Benton intermediate canopy), and NMT to plot UB-T (Upper Benton tall canopy). Other HRUs in the same tree height class used the same calibrated stomatal resistance values

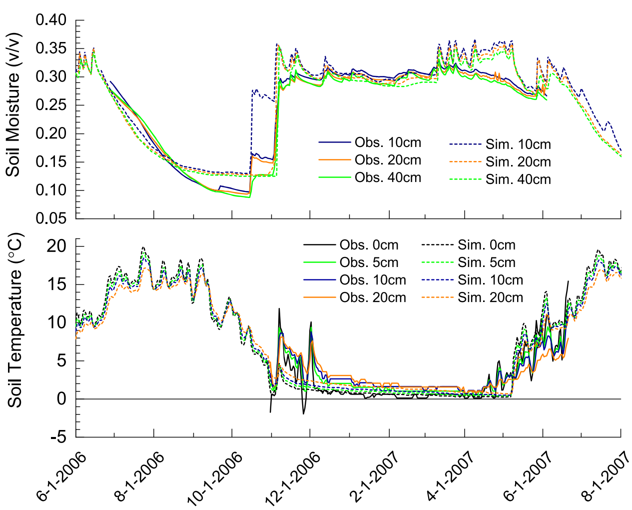

Figure 4. Observed and simulated daily mean soil moisture and temperature. Simulations were from HRU NMT. Observed temperature data were from one station within HRU NMT and observed soil moisture data were mean values across seven stations in PREF

precipitation at the different elevations. Mean annual transpiration was relatively consistent between HRUs, exhibiting a relatively narrow (~80 mm) range (Figure 7a) despite large differences in LAI (up to 5.2 $m^2 m^{-2}$, Table II). The two high elevation HRUs had the lowest transpiration. The ΔS was very similar among HRUs with a range of 12 mm (Figure 7d). As a result of these differences, the Q_{pot} ranged widely (213 mm) between HRUs. The two highest elevation HRUs (WHS and NHS) contributed much higher Q_{pot} than the low- and medium-elevation HRUs. In comparison, the differences in Q_{pot} were small among low- and medium-elevation HRUs (50 mm range) (Figure 7c).

DISCUSSION AND FUTURE DIRECTIONS

Agreement between simulated and observed snow and transpiration dynamics overall was very good, which is in part because of the parameterization process where default or measured parameters were refined to maximize model performance. Despite this success, there were some larger discrepancies in SWC and temperature that were likely related to errors in these terms. For example, the model underestimated soil temperature and moisture in November 2006 when air temperatures dropped below freezing and then warmed up dramatically (Figure 4). There was some rainfall during the cold period, which was simulated as snow because the temperature was lower than T_i in November 2006. In the SHAW simulation, simulated snow accumulated on the ground thereby limiting the heat transfer from air to soil, while in actuality the soil warmed up sharply because of the rise of air temperature. During this period, simulated snowmelt saturated the soil and produced higher soil moisture. Similarly, the model underestimated soil temperature and moisture for April–June, 2007, which may relate to the simulation of an earlier snowmelt than the observation during this time period (Figure 2).

Agreement between simulated potential and observed streamflow was very good at the annual scale, but there were also discrepancies at the intra-annual scale. Specifically, model simulations overestimated spring peak flow and underestimated low streamflows in summer through winter, thus reducing seasonal variations relative to observations (Figure 5a). This was related to the one-dimensional structure of the SHAW model, and the lack of a flow-routing algorithm. In a watershed, infiltrated water is routed to the stream channel via a range of flowpaths with different temporal lags including redistribution within the soil and bedrock profile, shallow subsurface lateral flow, and groundwater flow. Flow routing was not simulated in the one-dimensional HRU-based modelling approach. We hence directly compared

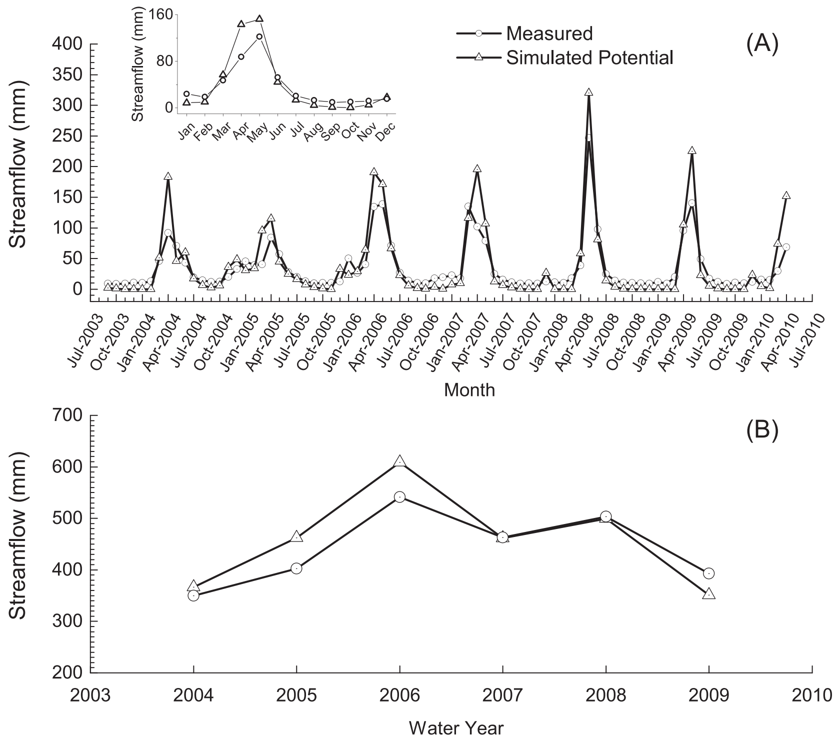

Figure 5. Simulated potential streamflow (Q_{pot}, runoff + deep drainage) and observed monthly and annual streamflow at Benton Dam. Inset shows the monthly ensemble mean streamflow

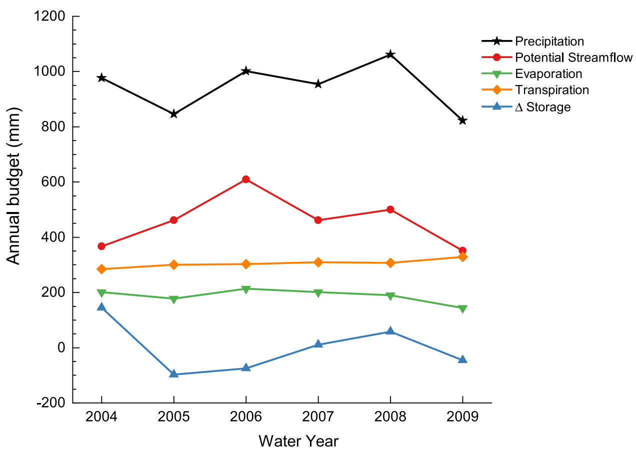

Figure 6. Inter-annual variation in simulated water budgets, compared to observed precipitation

measured Q to water exiting the lower boundary of the modelling domain plus a minor amount of overland flow (Q_{pot}). These differences were most pronounced during the seasonal snow ablation period as was expected. The simulated snowmelt quickly contributed to streamflow in the spring (March–May); whereas in actuality, snowmelt eventually reached the stream via a range of flowpaths with different temporal lags. This difference between simulated and observed Q was not unexpected, and similar flow lags were noted in similar applications of the model (Chauvin *et al.*, 2011), which emphasizes that this approach should not be used to estimate sub-annual streamflows, especially in basins with longer temporal flow lags.

Despite the limitations in simulating intra-annual hydrologic terms, the relatively simple approach of applying the SHAW model over a limited number of HRUs for Benton Basin produced reasonable results for components of the hydrological balance based on both internal observations and streamflow at the annual scale. In the basin water budget as shown in Equation (1), transpiration was the only minimally calibrated component, and precipitation was provided as an input. The simulations of Q_{pot}, which were not directly calibrated, were well matched with observed flows. As expected, precipitation was correlated with observed streamflow during the 6-year modelling period, because of relatively low interannual variations in evaporation, transpiration, and storage terms. The performance of the model given the minimal calibration suggests that it may be a promising approach to deconvolve the long-term combined hydrological effects of climate and vegetation changes in the watershed. Most notably, this approach may be used to understand the mechanisms that are responsible for long-term observed streamflow increases in the Benton Basin (Hatcher and Jones, 2013; Tinkham *et al.*, 2015), relative to declining flows throughout the region over a similar time period (Luce and Holden, 2009).

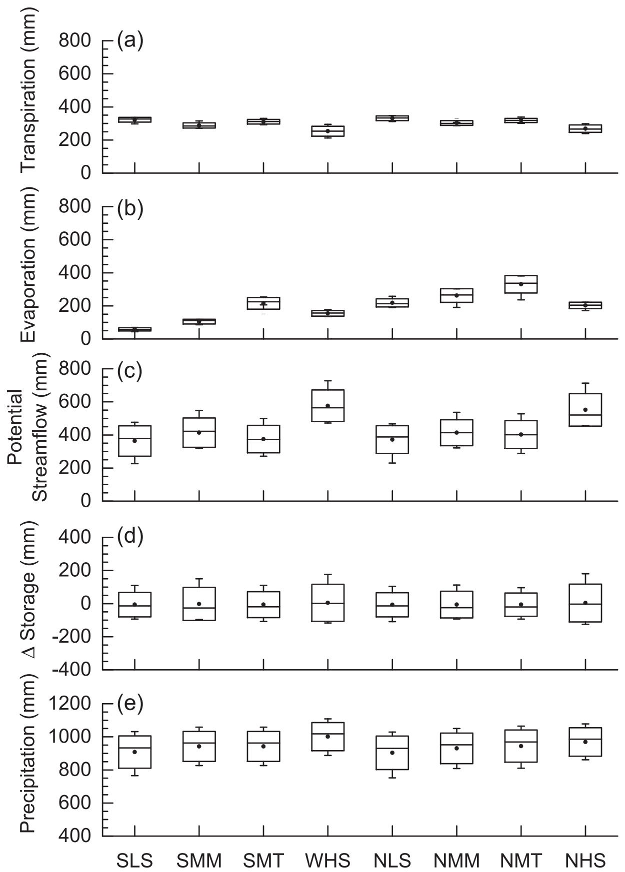

Figure 7. Variation in water budgets among HRUs in Benton Basin. Each box represents the mean from water year 2004 to 2009. The top and bottom whiskers show the maximum and minimum values among years respectively; three horizontal lines of the box show the 75%, 50% (median), and 25% percentiles of the six annual values; the dot in the box shows the mean. All y-axes have a range of 800 mm to facilitate visual comparisons between variables (see Figure 6 for abbreviations)

Application of the SHAW model as described in this manuscript but with historical vegetation coverage and inventory data as inputs would be a valuable tool to help understand why annual runoff is increasing in the Benton Basin despite opposite trends in larger basins throughout the region. The model can accurately simulate vegetation changes resulting from forest ageing, logging, and the observed replacement of western white pine by other species in PREF. The SHAW model simulations should help to estimate quantitatively the hydrological impacts of the vegetation changes. This is one example of how this implementation of the SHAW model with the regionalized parameter set can be applied to elucidate the mechanisms that have produced the observed increased streamflows from Benton Basin since 1939. While the increased streamflow may be a regional anomaly (Luce *et al*., 2013), it shows that hydrological responses to combined climate and vegetation changes may run counter to typical trends under specific circumstances. Physically based models like SHAW help to integrate complex ecological processes that affect the water cycle, while simple HRU-based approaches enable long-term simulations, so that we can more robustly evaluate potential effects of climate change on water budgets.

ACKNOWLEDGEMENTS

Funding was provided by the U.S. Forest Service Western Wildlands Environmental Threat Assessment Center (WWETAC) and to the University of Idaho through a Joint Venture Agreement (13-JV-11221633-130). Additional support was provided by the NASA New Investigator Program (NNX14AC26G). We thank Robert Denner for providing streamflow data, and Ina Sue Miller, Tom Black, and Charlie Luce for climate data.

REFERENCES

Abatzoglou JT. 2011. Influence of the PNA on declining mountain snowpack in the Western United States. *International Journal of Climatology* **31**: 1135–1142. DOI:10.1002/joc.2137.

Abatzoglou JT, Rupp DE, Mote PW. 2014. Seasonal climate variability and change in the Pacific Northwest of the United States. *Journal of Climate* **27**: 2125–2142.

Berghuijs WR, Woods RA, Hrachowitz M. 2014. A precipitation shift from snow towards rain leads to a decrease in streamflow. *Nature Climate Change* **4**(7): 583–586.

Berryman EM, Marshall JD, Kavanagh K. 2014. Decoupling litter respiration from whole-soil respiration along an elevation gradient in a Rocky Mountain mixed-conifer forest. *Canadian Journal of Forest Research* **44**: 432–440.

Campbell JL, Ollinger SV, Flerchinger GN, Wicklein H, Hayhoe K, Bailey AS. 2010. Past and projected future changes in snowpack and soil frost at the Hubbard Brook Experimental Forest, New Hampshire, USA. *Hydrological Processes* **24**: 2465–2480. DOI:10.1002/hyp.7666.

Chauvin GM, Flerchinger GN, Link TE, Marks D, Winstral AH, Seyfried MS. 2011. Long-term water balance and conceptual model of a semi-arid mountainous catchment. *Journal of Hydrology* **400**: 133–143. DOI:10.1016/j.jhydrol.2011.01.031.

Cline RG, Campbell GS, Haupt HF. 1977. Potential water yeld response following clearcut harvesting on north and south slopes in Northern Idaho.

Dai A. 2008. Temperature and pressure dependence of the rain-snow phase transition over land and ocean. *Geophysical Research Letters* **35**: L12802: . DOI:10.1029/2008gl033295.

Daly C, Neilson RP, Phillips DL. 1994. A statistical-topographic model for mapping climatological precipitation over mountainous terrain. *Journal of Applied Meteorology* **33**: 140–158. DOI:10.1175/1520-0450(1994)033<0140:astmfm>2.0.co;2.

Daly C, Taylor G, Gibson W. 1997. The PRISM approach to mapping precipitation and temperature. *Proceedings, 10th Conference on Applied Climatology, American Meteorology Society*, 10–12.

Du E, Link TE, Gravelle JA, Hubbart JA. 2014. Validation and sensitivity test of the distributed hydrology soil-vegetation model (DHSVM) in a forested mountain watershed. *Hydrological Processes* **28**: 6196–6210. DOI:10.1002/hyp.10110.

Duursma RA, Marshall JD, Robinson AP. 2003. Leaf area index inferred from solar beam transmission in mixed conifer forests on complex terrain. *Agricultural and Forest Meteorology* **118**: 221–236. DOI:10.1016/S0168-1923(03)00109-6.

Duursma R, Marshall J, Robinson A, Pangle R. 2007. Description and test of a simple process-based model of forest growth for mixed-species stands. *Ecological Modelling* **203**: 297–311.

Eskelson BN, Temesgen H, Lemay V, Barrett TM, Crookston NL, Hudak AT. 2009. The roles of nearest neighbor methods in imputing missing data in forest inventory and monitoring databases. *Scandinavian Journal of Forest Research* **24**: 235–246.

Fang X, Pomeroy J, Ellis C, MacDonald M, DeBeer C, Brown T. 2013. Multi-variable evaluation of hydrological model predictions for a headwater basin in the Canadian Rocky Mountains. *Hydrology and Earth System Sciences* **17**: 1635–1659.

Fekety PA, Falkowski MJ, Hudak AT. 2015. Temporal transferability of LiDAR-based imputation of forest inventory attributes. *Canadian Journal of Forest Research* **45**: 422–435. DOI: 10.1139/cjfr-2014-0405.

Finklin AI. 1983. Climate of the Priest River experimental forest, northern Idaho. General Tech. Rep. INT-159, USDA Intermountain Forest Range and Experimental Station, Ogden, UT; 58.

Flerchinger GN, Cooley KR. 2000. A ten-year water balance of a mountainous semi-arid watershed. *Journal of Hydrology* **237**: 86–99. DOI:10.1016/S0022-1694(00)00299-7.

Flerchinger G, Pierson F. 1991. Modeling plant canopy effects on variability of soil temperature and water. *Agricultural and Forest Meteorology* **56**: 227–246.

Flerchinger G, Saxton K. 1989a. Simultaneous heat and water model of a freezing snow–residue–soil system I. Theory and development. *Transaction of the ASAE* **32**: 565–571.

Flerchinger G, Saxton K. 1989b. Simultaneous heat and water model of a freezing snow–residue–soil system II. Field verification. *Transaction of the ASAE* **32**: 573–578.

Flerchinger G, Cullum R, Hanson C, Saxton K. 1990. Soil freezing and thawing simulation with the SHAW model. Frozen Soil Impacts on Agricultural, Range, and Forest Lands; 77–86.

Flerchinger GN, Hanson CL, Wight JR. 1996. Modeling evapotranspiration and surface energy budgets across a watershed. *Water Resources Research* **32**: 2539–2548. DOI:10.1029/96wr01240.

Flerchinger GN, Cooley KR, Hanson CL, Seyfried MS. 1998. A uniform versus an aggregated water balance of a semi-arid watershed. *Hydrological Processes* **12**: 331–342. DOI:10.1002/(sici)1099-1085(199802)12:2.

Flerchinger GN, Sauer TJ, Aiken RA. 2003. Effects of crop residue cover and architecture on heat and water transfer at the soil surface. *Geoderma* **116**: 217–233. DOI:10.1016/S0016-7061(03)00102-2.

Flerchinger GN, Reba ML, Link TE, Marks D. 2015. Modeling temperature and humidity profiles within forest canopies. *Agricultural and Forest Meteorology* **213**: 251–262. DOI:10.1016/j.agrformet.2015.07.007.

Gash JHC. 1979. An analytical model of rainfall interception by forests. *Quarterly Journal of the Royal Meteorological Society* **105**: 43–55. DOI:10.1002/qj.49710544304.

Hatcher KL, Jones JA. 2013. Climate and streamflow trends in the columbia river basin: evidence for ecological and engineering resilience to climate change. *Atmosphere-Ocean* **51**: 436–455. DOI:10.1080/07055900.2013.808167.

Hudak AT, Crookston NL, Evans JS, Hall DE, Falkowski MJ. 2008. Nearest neighbor imputation of species-level, plot-scale forest structure attributes from LiDAR data. *Remote Sensing of Environment* **112**: 2232–2245. DOI:10.1016/j.rse.2007.10.009.

Hudak AT, Strand EK, Vierling LA, Byrne JC, Eitel JUH, Martinuzzi S, Falkowski MJ. 2012. Quantifying aboveground forest carbon pools and fluxes from repeat LiDAR surveys. *Remote Sensing of Environment* **123**: 25–40. DOI:10.1016/j.rse.2012.02.023.

Kalra A, Piechota TC, Davies R, Tootle GA. 2008. Changes in US streamflow and western US snowpack. *Journal of Hydrologic Engineering* **13**: 156–163.

Kavanagh KL, Pangle R, Schotzko AD. 2007. Nocturnal transpiration causing disequilibrium between soil and stem predawn water potential in mixed conifer forests of Idaho. *Tree Physiology* **27**: 621–629. DOI:10.1093/treephys/27.4.621.

Kirchner JW. 2006. Getting the right answers for the right reasons: linking measurements, analyses, and models to advance the science of hydrology. *Water Resources Research* **42**. DOI:10.1029/2005wr004362.

Kumar M, Duffy CJ, Salvage KM. 2009. A second-order accurate, finite volume-based, integrated hydrologic modeling (FIHM) framework for simulation of surface and subsurface flow. *Vadose Zone Journal* **8**: 873–890.

Leyton L, Reynolds ERC, Thompson FB. 1967. Rainfall interception in forest and moorland. In *International Symposium on Forest Hydrology*, Sopper WE, Lull HW (eds). Pergamon Press: New York, USA; 163–178.

Link TE, Flerchinger GN, Unsworth M, Marks D. 2004a. Simulation of water and energy fluxes in an old-growth seasonal temperate rain forest using the simultaneous heat and water (SHAW) model. *Journal of Hydrometeorology* **5**(3): 443–457.

Link TE, Unsworth M, Marks D. 2004b. The dynamics of rainfall interception by a seasonal temperate rainforest. *Agricultural and Forest Meteorology* **124**: 171–191. DOI:10.1016/j.agrformet.2004.01.010.

Link TE, Wei L, Denner RJ. 2015. *Streamflow data for the Priest River Experimental Forest*. Fort Collins, CO: Forest Service Research Data Archive. DOI: 10.2737/RDS-2015-0006.

Luce CH, Holden ZA. 2009. Declining annual streamflow distributions in the Pacific Northwest United States, 1948–2006. *Geophysical Research Letters* **36**: L16401: . DOI:10.1029/2009gl039407.

Luce CH, Abatzoglou JT, Holden ZA. 2013. The missing mountain water: slower westerlies decrease orographic enhancement in the Pacific Northwest USA. *Science* **342**: 1360–1364. DOI:10.1126/science.1242335.

Marks D, Winstral A, Reba M, Pomeroy J, Kumar M. 2013. An evaluation of methods for determining during-storm precipitation phase and the rain/snow transition elevation at the surface in a mountain basin. *Advances in Water Resources* **55**: 98–110. DOI:10.1016/j.advwatres.2012.11.012.

Mote PW. 2003. Trends in temperature and precipitation in the Pacific Northwest during the twentieth century.

Ogink-Hendriks M. 1995. Modelling surface conductance and transpiration of an oak forest in The Netherlands. *Agricultural and Forest Meteorology* **74**: 99–118.

Page-Dumroese DS. 1993. Susceptibility of volcanic ash-influenced soil in northern Idaho to mechanical compaction. Reserch Note INT-409, USDA Forest Service INtermountain Research Station; 6.

Pangle RE. 2008. Transpiration and canopy conductance of mixed species conifer stands in an inland Pacific northwest forest. In Department of Forest Resources University of Idaho; 199.

Pangle R, Kavanagh K, Duursma R. 2015. Decline in canopy gas exchange with increasing tree height, atmospheric evaporative demand, and seasonal drought in co-occurring inland Pacific Northwest conifer species. *Canadian Journal of Forest Research* **45**: 1086–1101. DOI:10.1139/cjfr-2014-0551.

Smith WK, Young DR, Carter GA, Hadley JL, McNaughton GM. 1984. Autumn stomatal closure in six conifer species of the Central Rocky Mountains. *Oecologia* **63**: 237–242. DOI:10.1007/bf00379883.

Stage AR. 1957. Some runoff characteristics of a small forested watershed in northern Idaho. *Northwest Science* **31**: 14–27.

Thyer M, Beckers J, Spittlehouse D, Alila Y, Winkler R. 2004. Diagnosing a distributed hydrologic model for two high-elevation forested catchments based on detailed stand-and basin-scale data. *Water Resources Research* **40**: W01103. DOI:10.1029/2003WR002414.

Tinkham WT, Denner R, Graham RT. 2015. Climate, snowpack, and streamflow of priest river experimental forest revisited. U.S. Department of Agriculture, Forest Service, Rocky Mountain Research Station; 49.

Wallin G, Hall M, Slaney M, Räntfors M, Medhurst M, Linder S. 2013. Spring photosynthetic recovery of boreal Norway spruce under conditions of elevated [CO2] and air temperature. *Tree physiology* **33**(11): 1177–1191.

Walter MT, Wilks DS, Parlange JY, Schneider RL. 2004. Increasing evapotranspiration from the conterminous United States. *Journal of Hydrometeorology* **5**: 405–408.

Wei L, Marshall JD, Link TE, Kavanagh KL, Du E, Pangle RE, Gag PJ, Ubierna N. 2014. Constraining 3-PG with a new δ^{13}C submodel: a test using the δ13C of tree rings. *Plant, Cell & Environment* **37**: 82–100. DOI:10.1111/pce.12133.

Wigmosta MS, Nijssen B, Storck P, Lettenmaier D. 2002. The distributed hydrology soil vegetation model. Mathematical models of small watershed hydrology and applications; 7–42.

APPENDIX

Table A1. SHAW parameters for Benton Basin in PREF

Parameter (unit)			Value			Sources
Vegetation						
Characteristic dimension of leaves (cm)			0.2			Estimated
Rooting depth (m)			1.3			Estimated
Albedo of species			0.1			Estimated
Transpiration threshold (°C)			8.0			Calibrated
Min stomatal resistance for tree height classes		Tall	Medium	Short		Calibrated
(s m^{-1})		420	410	260		
Resistance function exponent			5			Default
Critical leaf water potential			−200			Estimated
Leaf resistance (kg m^{-3} s^{-1})			1×10^5			Default
Root resistance (kg m^{-3} s^{-1})			2×10^5			Default
Maximum interception per unit leaf area (mm)			0.31			Observed
K_{VPD} in VPD response Equation (2)			0.10			Observed
r in VPD response Equation (2)			0.36			Observed
Snow properties						
Maximum temperature for snow (°C)			0			Calibrated
Roughness length (cm)			0.15			Default
Residue properties						
Fraction of surface covered (%)			100			Estimated
Albedo of residue			0.25			Default
Dry mass of residue (kg ha^{-1})			9000			Estimated
Thickness of residue (cm)			8			Estimated
Litter resistance to vapour transport (s m^{-1})			50 000			Default
Soil properties						
Saturated conductivity (cm h^{-1})			2			Calibrated
Air-entry potential (m)			−0.02			Calibrated
Pore-size distribution index			8			Calibrated
Depth of layer (cm):	*0–10*	*10–30*	*30–50*	*50–70*	*>70*	
Sand/silt/clay (% by weight)	50/45/5	44/49/7	50/43/7	58/35/7	63/31/6	Measured
Organic matter content (% by weight)	3.19	1.10	0.50	0.27	0.20	Measured
Depth of layer (cm):	*0–120*	*140*	*160*	*180*	*200*	
Rock content (% by weight)	0	10	20	30	40	Estimated
Depth of layer (cm):	*0–10*	*10–20*	*20–40*		*>40*	
Bulk density (kg m^{-3})	670	800	980		1050	Measured
Saturated volumetric moisture content ($v\ v^{-1}$)	0.44	0.43	0.42		0.41	Measured